Hindawi Publishing Corporation
International Journal of Rotating Machinery
Volume 2007, Article ID 56808, 15 pages
doi:10.1155/2007/56808

Research Article

Active Suppression of Rotating Stall Inception with Distributed Jet Actuation

Huu Duc Vo

Département de génie mécanique, École Polytechnique de Montréal, Campus Université de Montréal, 2900 boulevard Édouard-Montpetit, 2500 chemin de Polytechnique, bureau C318.9, Montréal, Québec, Canada H3T 1J4

Received 19 October 2006; Accepted 5 March 2007

Recommended by Meinhard T. Schobeiri

An analytical and experimental investigation of the effectiveness of full-span distributed jet actuation for active suppression of long length-scale rotating stall inception is carried out. Detailed modeling and experimental verification highlight the important effects of mass addition, discrete injectors, and feedback dynamics, which may be overlooked in preliminary theoretical studies of active control with jet injection. A model of the compression system incorporating nonideal injection and feedback dynamics is verified with forced response measurements to predict the right trends in the movement of the critical pole associated with the stall precursor. Active control experiments with proportional feedback control show that the predicted stall precursors are suppressed to give a 5.5% range extension in compressor flow coefficient. In addition, results suggest that the proposed model could be used to design a more sophisticated controller to further improve performance while reducing actuator bandwidth requirements.

1. INTRODUCTION

Aerodynamic instabilities in axial compressors, in the form surge and rotating stall, are among the main limiting factors in efficiency improvement of current gas turbine engines. Surge is a high-amplitude axisymmetric oscillation of the flow across the compressor (and gas turbine). Rotating stall features the formation of a circumferentially nonuniform velocity disturbance rotating at a fraction of the rotor speed, with a large drop in pressure ratio. Surge is often triggered by rotating stall. Both are detrimental to the performance and durability of the compressor. Attempts to avoid them by setting of an operational safety margin often do so at the expense of efficiency, by positioning the operating point further from the point of maximum efficiency. A modern solution pursued by researchers over the past few years is to actively suppress the aerodynamic instabilities with feedback control and extend the compressor's operating range. However, its implementation requires an understanding of these instabilities.

There are two well-established routes to rotating stall, referred to as long length-scale or "modal" stall inception and short length-scale or "spike" stall inception, distinguished by the type of initial perturbation in pressure/velocity.

First described by Day [1], short length-scale stall inception is characterized by the appearance of a local disturbance (or "spike") two to three blade pitches in width at the rotor tip and whose associated velocity defect is comparable to the mean velocity through the compressor. The spike rotates at about 70% of the rotor speed and can grow into a full-span circumferentially two-dimensional stall cell within only roughly three rotor revolutions. This type of stall inception has not been well understood. As a result, only passive empirical stabilization techniques have been applied in these cases, such as discrete tip microair injection by Nie et al. [2]. Recently, Vo et al. [3] proposed two criteria linked to tip clearance flow to explain and predict the formation of spike disturbances. However, reduced-order models both for the formation and growth of the disturbance, which would be very useful for the design of active control systems, do not yet exist. In addition, the localized and limited extent of the disturbance, as well as its very rapid growth rate into a fully developed rotating stall cell makes early detection and real-time active suppression rather difficult to achieve.

In contrast, long length-scale, or modal stall inception, is characterized by the evolution, in tens of rotor revolutions, of a small amplitude full-span ("modal") disturbance (stall precursor) with wavelength on the order of the annulus

circumference rotating at around 30–40% of rotor speed into a fully developed stall cell. These features have many important implications for active stabilization of modal stall inception. First, the small amplitude, full-span extent, and long (circumferential) wavelength of the modal disturbance implies that linearized models which consider the overall effects of the blading, rather than the details of the flow on the blade scale, can be used. This has been successfully implemented with the actuator disk approach by Moore [4] and Moore and Greitzer [5]. The resulting Moore-Greitzer model can be used to predict and optimize the effectiveness of active control schemes. Second, linearization allows the spatially periodic disturbance to be decomposed into independent circumferential spatial harmonics, which can be stabilized separately, thus facilitating the task of control. Last but not least, the large spatial extent of the modal disturbance means that the stall precursor can be easily detected and its relatively low-growth rate and small amplitude imply that small disturbance generators can be used in time to prevent its growth into fully developed rotating stall.

Active suppression of modal stall inception was first implemented by Paduano et al. [6] on a single-stage low-speed axial compressor using a set of 12 independently moving inlet servo guide vanes (SGVs) and constant feedback control capable of controlling the first three harmonics. Paduano was able to extend the compressor operating range by 23% in terms of the stalling flow coefficient. Haynes et al. [7] applied the same technique on a three-stage low speed axial compressor and improved its range by 7.8%. Van Schalkwyk et al. [8] added inlet distortion to Haynes' experiment and extended the operating range by 3.7% for an inlet distortion of 0.8 dynamic head covering 180° of the compressor annulus. However, a theoretical comparison by Hendricks and Gysling [9] of the effectiveness of different sensor-actuator schemes suggests distributed jet actuators could give the largest range extension and the lowest rotational frequency of the prestall disturbance (i.e., the least demanding in terms of actuator bandwidth) for the same feedback gain values. Tip jet injection with aeromechanical feedback was explored on a single-stage low speed compressor by Gysling and Greitzer [10]. Subsequently, discrete tip injection was tested with feedback control on a high-speed single stage compressor by Weigl et al. [11], and the nature of this tip injection was later investigated by Suder et al. [12]. Actively controlled discrete midspan pulsed injection with only three injectors has been carried out by D'Andrea et al. [13] on a small single stage compressor to remove the hysteresis in the compressor pressure rise characteristics (speedlines) that is usually associated with rotating stall. Although other recent studies have been exploring active control with other actuation schemes, such as bleed valves (Yeung et al. [14]), magnetic bearings for tip clearance control (Spakovszky et al. [15]), and dynamic adjustment of stator stagger angle (Schobeiri and Attia [16]), another extensive comparative theoretical study by Fréchette et al. [17] of different actuation schemes again point to jet injection as the most promising for rotating stall control. However, no attempt has yet been done to experimentally verify the concept of active control using full-span circumferentially continuous (distributed) jet injection, as proposed by Hendricks and Gysling [9]. The objective of this research is to assess the true effectiveness of active suppression of modal stall inception using full-span distributed jet actuation on a multistage compressor through detailed modeling and experimentation. A part of this work, focusing on the model, was reported by Vo and Paduano [18].

First, a brief description of the experimental apparatus is given. Thereafter, an idealized jet injection model is derived and integrated into a model of the compression system, whose verification with test data leads to the formulation of an empirical model of the real injectors. Simulations performed with different levels of modeling complexity reveal the dominant effects of injection and feedback dynamics. Third, system identification experiments are done to validate the final complete system model. Finally, active control experiments are carried out to assess the effectiveness of this actuation, and the results and observations are compared with theoretical predictions.

2. EXPERIMENTAL APPARATUS

The MIT low-speed three stage axial compressor facility used in this research was designed by Eastland [20] using a Pratt & Whitney research compressor. It has a constant tip diameter of 610 mm, a constant hub-to-tip ratio of 0.88, and it operates at 2400 rpm. Further details of the compressor can be found in Haynes et al. [7]. This compressor has been extensively used in stall research, starting with Gamache and Greitzer [21] who measured reversed-flow performance and later by Garnier et al. [22] who confirmed the presence of modal disturbances prior to rotating stall. This led to the use of this compressor in active rotating stall stabilization research by Haynes et al. [7] and Van Schalkwyk et al. [8]. The facility was subsequently modified by Vo and Paduano [18] for experimental research with jet injection. A side view and cross-section of the compression system are shown in Figure 1. The compressor, driven by an electric motor with a tachometer and a torque sensor, draws air through a bellmouth inlet and two coarse screens. A set of eight pitot probes and 16 circumferentially equally spaced hot wires are placed at the midspan of the annulus upstream of the inlet guide vanes (IGVs) for time-averaged and unsteady velocity measurements, respectively. An actuator ring is sandwiched between the IGVs and first rotor as shown in Figure 1. Time-averaged inlet total and exit static pressure measurements are obtained through the pitot probes and compressor exit endwall static pressure taps, respectively. The air exiting the compressor enters a small annular exhaust plenum and passes through a conical valve used as a throttle to control the mass flow (and thus the flow coefficient). The plenum volume is small enough to preclude surge. The air subsequently exits outdoors via a dump plenum and a duct with several screens and an orifice plate, for mass flow measurement (to obtain flow coefficient).

For active control with jet actuation, the servo guide vanes used previously were replaced by twelve jet actuators designed by Diaz [19]. Each jet actuator consists of a valve

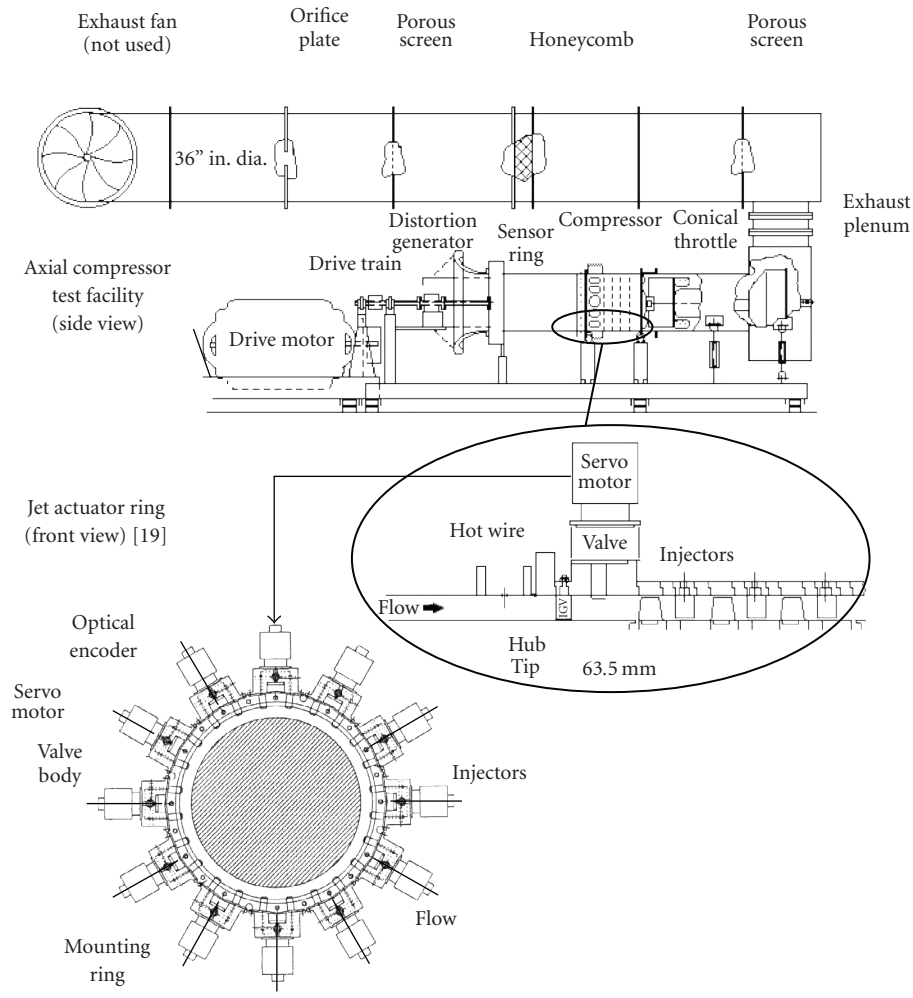

Figure 1: MIT low-speed three-stage axial compressor test facility with jet actuation.

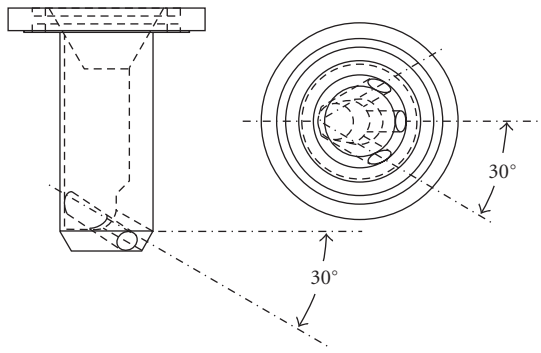

Figure 2: Injector design [19].

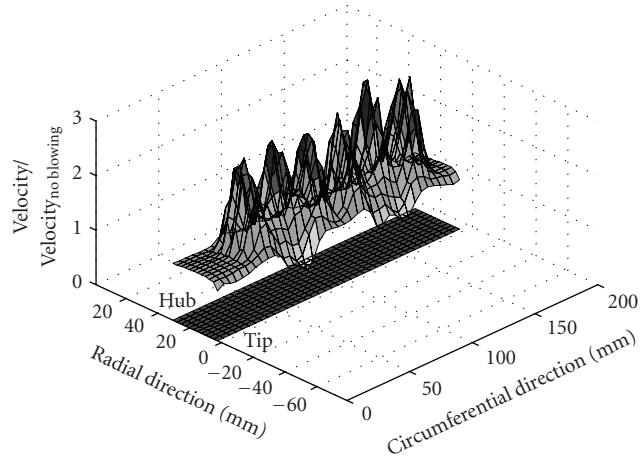

Figure 3: Measured velocity profile at relative axial location of first rotor face for steady injection with two injectors at 14.8% of stall mass flow through section incorporating 1/12 of unwrapped compressor annulus [19].

and two "shower head" injectors. Each injector (see Figure 2) has three 3/16 in. dia. holes pointed 30° into the flow and 30° from each other to give as complete and uniform a radial and circumferential coverage as possible as shown by the velocity profile in Figure 3, with injection measured in a wind tunnel.

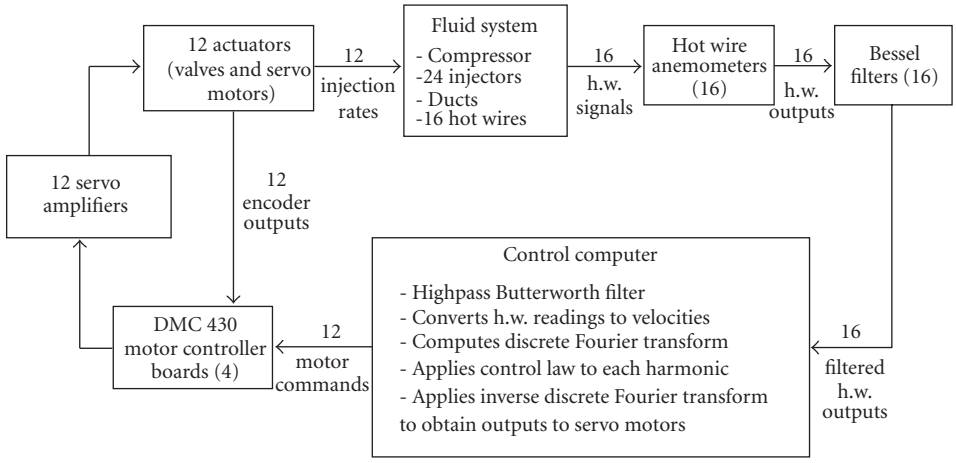

Figure 4: Closed-loop control feedback configuration.

Figure 4 presents a schematic description of operation of the overall system with closed-loop control. The sixteen hotwires upstream of the compressor detect modal stall disturbances. Their filtered signals serve to construct a picture of the rotating circumferential velocity disturbance in the control computer, which then decomposes this disturbance into the first three spatial harmonics by discrete Fourier transformation. A control law, in this case a constant gain and phase shift, is applied to each spatial harmonic to be controlled. The resulting commanded actuated disturbance to produce is obtained by inverse discrete Fourier transformation, and translated into the signals to send to each of the twelve jet actuators. The actuators operate at a common mean injection mass flow and the signals modulate the injection around this mean mass flow. The next section will present an analytical model of this system.

3. SYSTEM MODELLING AND THEORETICAL PREDICTIONS

The following section describes the model of the compression system from the inlet duct to the exit duct starting with the derivation of the jet actuator model followed by its integration into the model of the compression system. A model of the feedback dynamics associated with the control system is also incorporated. Experimental data is then taken to verify and correct the injection model with an empirical model for the real injectors. Subsequently, the theoretical stall predictions with closed-loop control based on increasing modeling complexity are presented.

The general assumptions associated with the compression system model are the same as that used by Haynes et al. [7] including small disturbances (linearity), two-dimensionality (no radial variation of flow parameters) and incompressibility of the flow, a semiactuator disk representation of the compressor, and long enough ducting upstream and downstream for pressure disturbances to die out.

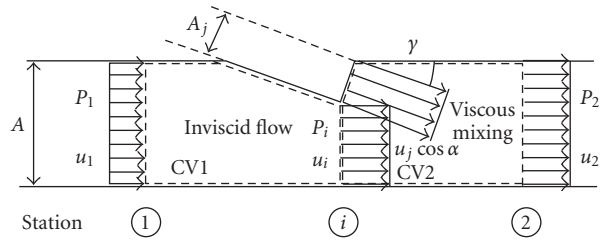

Figure 5: Control volume analysis of the modeled jet actuator.

However, additional modeling assumptions are required for the derivation of the theoretical injection model. First, the 24 discrete injectors between the IGVs and first blade row (see Figure 1) are replaced by one circumferentially continuous injector of equal total injection area placed upstream of the IGVs as shown in Figure 5. Instead of injecting at the IGV exit circumferential flow angle (α) and at a 30° radial angle, the modeled injector points axially with an effective axial injection velocity proportionately reduced by $\cos\alpha$, and injects at a radial angle (γ) whose value is chosen to give the equivalent axial momentum transfer to that of the actual discrete jet injectors. By its circumferentially continuous nature, the modeled injector can put in perfect annular sine wave disturbances. Diaz [19] gave an indication of how close the set of 24 discrete injectors can come to satisfying this assumption. Second, from Figure 5, it is assumed that no losses occur between stations 1 and i, and that total mixing occurs between stations i and 2. Finally, the distance between stations 1 and 2 is assumed to be short enough for the associated fluid inertia effects to be neglected.

3.1. Injector model

A control volume analysis of the jet actuator modeled in Figure 5 yields the following equations.

From station 1 to station i:

continuity

$$\rho u_i A_i = \rho u_1 A \quad (A_i = A - A_j \cos\gamma). \tag{1}$$

Bernoulli

$$P_i + \frac{1}{2}\rho u_i^2 = P_1 + \frac{1}{2}\rho u_1^2. \tag{2}$$

From station i to station 2 (CV2):

continuity

$$\rho u_2 A = \rho u_j \cos\alpha A_j + \rho u_i A_i. \tag{3}$$

Axial momentum

$$(P_i - P_2)A = -\rho u_i^2 A_i - \rho u_j^2 \cos^2\alpha A_j \cos\gamma + \rho u_2^2 A. \tag{4}$$

The second term on the right-hand side of (4) represents the effect of momentum addition, whereas the other two terms are the effect of mass addition. Combining (1) through (4), then simplifying and nondimensionalizing gives

$$\phi_2 = \phi_1 + \left(\frac{A_j}{A}\cos\alpha\right)\phi_j, \tag{5}$$

$$\frac{P_{t2} - P_{t1}}{\rho U^2} = -\frac{1}{2}M\phi_2^2 - (N\cos\alpha)\phi_2\phi_j + \frac{1}{2}(R\cos^2\alpha)\phi_j^2, \tag{6}$$

where $R \equiv (A_j/A)(2\cos\gamma + N)$,

$$M \equiv \left(\frac{(A_j/A)\cos\gamma}{1 - (A_j/A)\cos\gamma}\right)^2,$$
$$N \equiv \frac{(A_j/A)\left(1 - 2(A_j/A)\cos\gamma\right)}{\left(1 - (A_j/A)\cos\gamma\right)^2}, \tag{7}$$

which in linearized form are

$$\delta\phi_2 = \delta\phi_1 + \left(\frac{A_j}{A}\cos\alpha\right)\delta\phi_j, \tag{8}$$

$$\frac{\delta P_{t2} - \delta P_{t1}}{\rho U^2} = -X\delta\phi_2 - Y\delta\phi_j, \tag{9}$$

where $X \equiv M\overline{\phi}_2 + N\overline{\phi}_j\cos\alpha$, $Y \equiv (N\overline{\phi}_2 - R\overline{\phi}_j\cos\alpha)\cos\alpha$.

3.2. Fluid system model

As explained in detail in [18], the fluid system model is obtained essentially by adding the pressure rise across the actuator (9) to the pressure rise across the compressor, as given by the Moore-Greitzer model with unsteady losses [7, 9, 23, 24], and combined with the model's irrotational/incompressible/inviscid upstream and incompressible/inviscid downstream flow fields. The resulting equations of the combined fluid system can be Fourier decomposed to give the following ordinary differential equations for the Fourier coefficients for each spatial circumferential harmonic (n):

$$\begin{aligned} k\dot{\widetilde{\phi}}_n = {} & \left(\frac{d\psi_i}{d\phi} - X + in\lambda\right)\widetilde{\phi}_n - e^{n\eta_{hw}}\widetilde{L}_{uSn} - e^{n\eta_{hw}}\widetilde{L}_{uRn\,jn} \\ & + e^{n\eta_{hw}}\left[\left(\frac{d\psi_i}{d\phi} - X + in\lambda\right)\frac{A_j}{A}\cos\alpha - Y\right]\widetilde{\phi}_{jn} \\ & - e^{n\eta_{hw}}\left[\left(\frac{1}{n} + \mu\right)\frac{A_j}{A}\cos\alpha\right]\dot{\widetilde{\phi}}_{jn}, \end{aligned} \tag{10}$$

$$\tau_S\dot{\widetilde{L}}_{uSn} = \left(\frac{dL_{uS,ss}}{d\phi}e^{-n\eta_{hw}}\right)\widetilde{\phi}_n - \widetilde{L}_{uRn} + \left(\frac{dL_{uS,ss}}{d\phi}\frac{A_j}{A}\cos\alpha\right)\widetilde{\phi}_{jn}, \tag{11}$$

$$\begin{aligned} \tau_R\dot{\widetilde{L}}_{uRn} = {} & \left(\frac{dL_{uR,ss}}{d\phi}e^{-n\eta_{hw}}\right)\widetilde{\phi}_n - (1 - in\tau_R)\widetilde{L}_{uRn} \\ & + \left(\frac{dL_{uR,ss}}{d\phi}\frac{A_j}{A}\cos\alpha\right)\widetilde{\phi}_{jn} \end{aligned} \tag{12}$$

$$\tau_a\dot{\widetilde{\phi}}_{jn} = \widetilde{\phi}_{jcn} - \widetilde{\phi}_{jn}, \tag{13}$$

where $k \equiv (2/n) + \mu$ $(n > 0)$.

Equation (13) represents the delay due the convection time lag of the jet from the actuator valve slit to the compressor face, modeled as a first order lag.

Finally, the temporal Laplace transform of (10) to (13) is taken and the four equations can be solved to give the desired transfer function for the spatial Fourier coefficient (SFC) of each harmonic (n):

$$\frac{\widetilde{\phi}_n(s)}{\widetilde{\phi}_{jcn}(s)} = \frac{G's + B' - \dfrac{C'L_{uRj}}{1 - in\tau_R + \tau_R s} - \dfrac{C'L_{uSj}}{1 + \tau_S s}}{\left(s - A' + \dfrac{C'L_{uR\phi}}{1 - in\tau_R + \tau_R s} + \dfrac{C'L_{uS\phi}}{1 + \tau_S s}\right)(\tau_a s + 1)}, \tag{14}$$

where

$$\begin{aligned} L_{uR\phi} &\equiv \frac{dL_{uR,ss}}{d\phi}e^{-n\eta_{hw}}, \qquad L_{uRj} \equiv \frac{dL_{uR,ss}}{d\phi}\frac{A_j}{A}\cos\alpha, \\ L_{uS\phi} &\equiv \frac{dL_{uS,ss}}{d\phi}e^{-n\eta_{hw}}, \qquad L_{uSj} \equiv \frac{dL_{uS,ss}}{d\phi}\frac{A_j}{A}\cos\alpha, \\ A' &\equiv \frac{1}{k}\left(\frac{d\psi_i}{d\phi} - X + in\lambda\right), \\ G' &\equiv -\frac{e^{n\eta_{hw}}}{k}\left(\frac{1}{n} + \mu\right)\frac{A_j}{A}\cos\alpha, \\ B' &\equiv \frac{e^{n\eta_{hw}}}{k}\left[\left(\frac{d\psi_i}{d\phi} - X + in\lambda\right)\frac{A_j}{A}\cos\alpha - Y\right], \\ C' &\equiv \frac{e^{n\eta_{hw}}}{k}. \end{aligned} \tag{15}$$

3.3. Modeling of control system dynamics

The theoretical study by Hendricks and Gysling [9] employs direct feedback on a model of the fluid system similar to the one derived above. However, to better predict the performance of actuation in practice, one should incorporate all the dynamics associated with the feedback loop. In this case, the pertinent control system dynamics are the feedback time delay, the highpass filters, the sample and hold dynamics of the discrete control process and the actuator dynamics. These dynamics, with the exception of the highpass filter, were modeled in detail by Haynes et al. [7], although some aspects are modified here to account for changes in the system.

First, the total feedback time delay from the velocity disturbance at the compressor face to the commanded actuation sent to the servo motors can be lumped and modeled by a pure time delay whose first order approximation is (16). Second, the only filter whose dynamics can significantly affect the system is a first-order Butterworth highpass filter with a cutoff frequency (f) of 0.1 Hz. It was used to correct for the drift of the hot wires during the experiments. The filter was implemented in the computer software and can be modeled by (17). Third, the sample and hold dynamics of the discrete-time control system was modeled in continuous time by Haynes [24] as (18). Finally, the actuator dynamics incorporate the dynamics from the commanded to actual servo motor position. This is modeled with the measured transfer function in (19):

$$D(s) = \frac{1 - (\tau_t/2)s}{1 + (\tau_t/2)s}, \tag{16}$$

$$F(s) = \frac{s}{s + 2\pi f R/U}, \tag{17}$$

$$\mathrm{ZOH}(s) = \frac{1}{1 + (\tau_f/2)s}, \tag{18}$$

$$A(s) = \frac{(s + 1.1934)(s + 0.3869 \pm i0.3443)}{(s + 0.1824 \pm i0.2933)(s + 1.5971 \pm i3.0352)} \bullet \frac{(s - 3.2229 \pm i1.8607)}{(s + 3.2229 \pm i1.8607)}. \tag{19}$$

To complete the model, the values of the parameters need to be obtained. Some, such as fluid inertias, can be calculated from geometry. Others were obtained empirically. Such is the case for the isentropic and actual compressor speedlines. The former is derived from the torque input and compressor velocity, the latter from pressure measurements. The difference between them is the total fluid loss L_u, with $L_{R,ss} = rL_u$ and $L_{S,ss} = (1 - r)L_u$, where r is the reaction of the compressor.

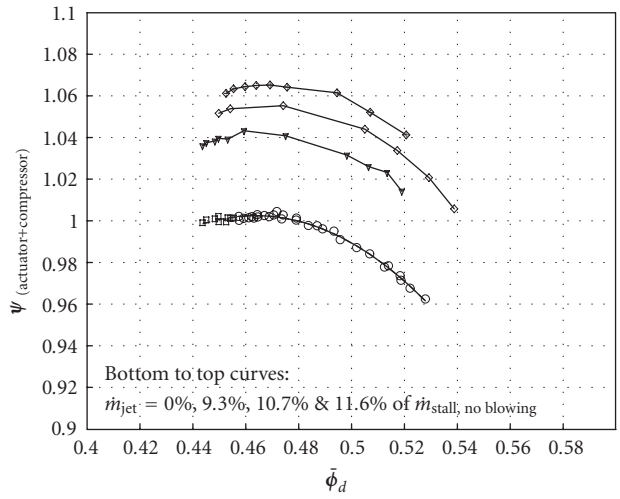

Figure 6: Actuator/compressor characteristics at several mean injection rates with closed-loop control (lowest solid line is fit of speedline for baseline case).

The values of the parameters are

$$\psi = -9.9222\phi^2 + 9.2018\phi - 1.1310 \quad (0.443 \le \phi \le 0.528),$$

$$\psi_i = -0.5467\phi^2 - 1.6328\phi - 2.0400 + \frac{0.1173}{\phi} \quad (0.458 \le \phi \le 0.528),$$

$$r = 0.75, \quad \lambda = 0.6787, \quad \mu = 1.2937, \quad \eta_{\mathrm{hw}} = -0.6034,$$

$$\tau_R = 0.177/\overline{\phi}_d, \quad \tau_S = 0.162/\overline{\phi}_d, \quad \alpha = 8.2^\circ, \quad \gamma = 37.9^\circ,$$

$$\frac{A_j}{A} = 0.0197, \quad \tau_a = 0.6132, \quad \tau_t = 0.248, \quad \tau_f = 0.503. \tag{20}$$

3.4. Experimental verification of injection model

Total-to-static pressure rise speedlines across the actuator/compressor at several injection rates were measured to verify the injection model, as shown in Figure 6. The circular points on the baseline (bottom) curve are measured without injection, nor active control. For nonzero mean injection rates, closed-loop control is applied in order to get pressure rise characteristics down to the lowest possible flow coefficient without stalling. It must be noted that since the injected jet is modulated around a mean value, the farther the mean injection rate is from a mid-value, the lower is the control gain without saturating the actuators, which explains the lower flow range extension for the speedlines with higher mean mass flow. In Figure 6, by subtracting the baseline case (zero injection) from the other curves in the stable baseline flow range ($\overline{\phi}_d > 0.458$), the effect of injection can be extracted as shown in Figure 7. These effects can then be subtracted from the speedlines with mean injection in the unstable flow range ($\overline{\phi}_d \le 0.458$) to deduce the (unmeasured)

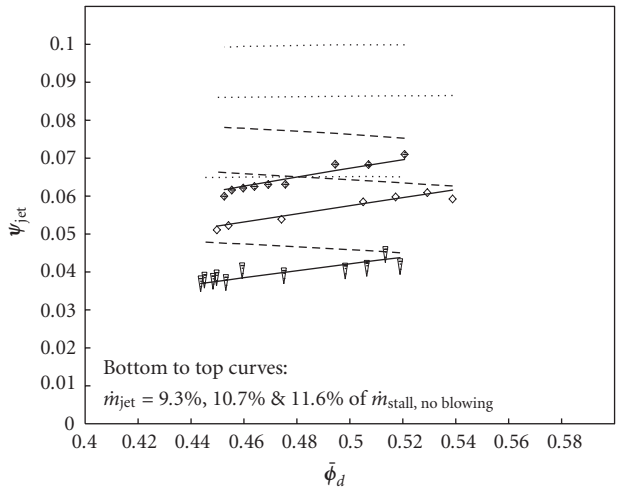

FIGURE 7: Jet contribution (ψ_{jet}) to $\psi_{(actuator + compressor)}$ (points) and fit (solid lines) versus full-mixing model (dashed lines) and pure momentum addition model (dotted lines).

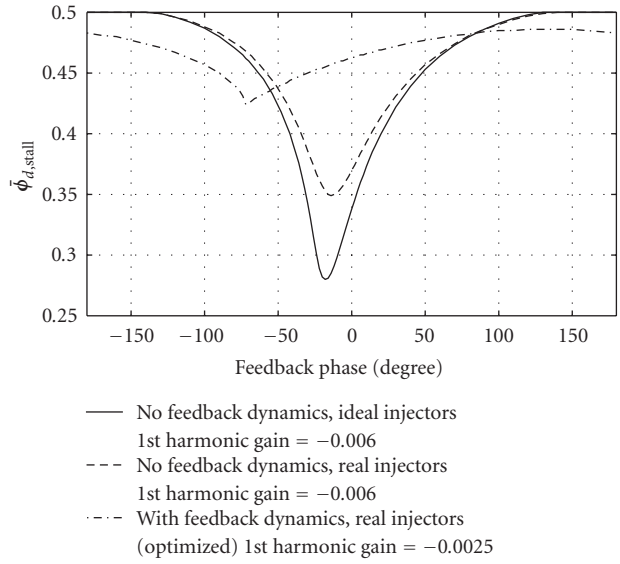

FIGURE 8: Theoretical predictions of the downstream flow coefficient at stall for first spatial harmonic control with an optimum feedback gain and varying feedback phase for various levels of modeling.

square points on the baseline curve in Figure 6. Figure 7 also shows the corresponding prediction of the injection model described by (6) (dashed line) as well as that of a model which solely incorporates the momentum addition term in (4) (dotted line).

Two important observations on the effectiveness of jet injectors can be made from Figure 7. First, by comparing the dashed lines with the corresponding dotted lines, one can see that the effect of mass addition is to significantly reduce the stagnation pressure rise of the injector (ψ_{jet}) (approximately 25% in this case). Second, the experimental results, which are obtained with discrete actuators and incomplete mixing, have slightly positive slope with mass flow, while the theory shows negative slope, implying a reduction in actuation effectiveness with decreasing flow coefficient. This is a relatively small effect that may be associated with incomplete mixing of the discrete actual jets with the background flow. An empirical model of jet injection is obtained by curve fitting the data points, as shown by the solid lines in Figure 7, which gives the following experimental (empirical) nonideal injection model:

$$\frac{P_{t2} - P_{t1}}{\rho U^2} = a\phi_j^2 + b\phi_j + c\phi_j\phi_2 + d\phi_2 + e\phi_2^2, \tag{21}$$

where $a = 0.0119$, $b = -0.0259$, $c = 0.0429$, $d = 1\text{E-}4$, $e = -2\text{E-}4$.

3.5. Theoretical stall predictions

The system model set up previously is used here to predict the stall point of the MIT three-stage compressor with proportional feedback control. Three different levels of modeling are used to evaluate the potential effect of nonideal injection and feedback dynamics on the performance of the closed-loop system. The first configuration has idealized injectors described by (6) but without feedback dynamics, that is, feedback is done directly on (14). This is similar to the configuration used in the study by Hendricks and Gysling [9]. The second configuration uses the real injectors represented by (21). The last configuration adds feedback dynamics to the control loop, thus incorporating (14) through (19) in the loop depicted in Figure 4. The controller uses simple proportional control ($K_n e^{i\beta_n}$) with constant gain (K_n) and phase shift (β_n) for each spatial harmonic (n).

Figure 8 shows the lowest attainable flow coefficient predicted for first spatial harmonic control with optimum gain and varying phase, using the different models. The effect of nonideal injection (solid versus dashed lines) is a reduction in range extension by about the same proportion as the reduction in pressure rise due to the jet (see Figure 7), without modifying the phase optimization curve of the system. At a fixed ideal phase, simulations (not shown) indicate that the stall flow coefficient continuously decreases with increasing gain. However, the addition of the feedback dynamics not only causes another sharp drop in flow range extension but alters the behavior of the system. First, the dashed-dotted curve in Figure 8 shows that the optimum phase value has been shifted from the cases without feedback dynamics. Second, at a fixed ideal phase value, a minimum stall coefficient is reached at a finite gain value of approximately −0.0025, as indicated in the legend of Figure 8.

These observations suggest that nonideal injection and feedback dynamics, especially the latter, can have a severe impact on the performance of the control system with jet actuators. Thus, these effects should be included in any predictions of closed-loop system performance and control law design with jet actuation.

4. SYSTEM IDENTIFICATION

System identification experiments were carried out to verify the accuracy of the model of the compression system with nonideal injection and feedback dynamics. This is done by comparing the theoretical and experimental root locus of the system, with particular focus on the critical pole, that is, pole associated with the stall precursor. The distance of this pole along the negative real axis of the root locus plot represents the damping of the associated stall precursor, and its distance along the imaginary axis represents the rotational speed of the stall precursor as a fraction of the rotor speed. Both open-loop and closed-loop comparisons are made for varying flow coefficient and control feedback gain and phase.

4.1. Identification methodology

The system identification runs were performed using an input temporal frequency sweep from 0 to 100 Hz on the amplitude of a stationary spatial cosine injection wave for one harmonic at a time. The temporal variation of the corresponding harmonic, in the form of the coefficients of the spatial cosine and sine waves, is computed from the hot-wire measurements. The output of the system contains both positive and negative frequencies, which represent clockwise (rotor direction) and counter clockwise rotational disturbances. The transfer functions from commanded SFC (spatial Fourier coefficient) to measured SFC for each harmonic are computed over the frequency domain of interest and fitted using Matlab with the coherence used as a weighting factor in the fit. The poles and zeros derived from the fitted transfer functions are plotted along with the theoretical poles and zeros calculated for the same operating parameters using the system's model.

4.2. Identification results

The open-loop system identification results for varying flow coefficient for the first harmonic are shown in Figure 9, with the corresponding plot for the closed-loop system in Figure 10. The corresponding root loci for the second and third harmonics show the same trends (reduced damping with decreasing flow coefficient) and thus are not shown. The root loci with varying gain and phase for the first and second spatial harmonics are shown in Figures 11 through 14. Results for the third spatial harmonic (not shown) present similar trends, but had lower coherence. Some features on these root locus plots need to be explained. First, (critical) poles that are associated with the stall precursor are enclosed by a box with solid lines. Second, the large arrows close to groups of poles indicate the direction of decreasing flow coefficient, increasing gain or decreasing phase, depending on the root locus plot under consideration. Third, the flow coefficient, feedback gain, and phase values are indicated on the figures.

The root loci with variation in flow coefficient, illustrated in Figures 9 and 10, show that the model well captures the stall precursor pole in terms of rotational frequency for the first spatial harmonic, but Figure 9 suggests that it may overestimate its damping. Corresponding root loci for the second and third harmonics show the same results. As for the closed-loop case with varying gain, Figure 11 shows that the general trajectory of the first harmonic precursor pole is fairly accurately predicted, showing the fact that active control with constant gain feedback moves the first harmonic precursor pole into the undesirable zone of higher frequency for this system. However, it is observed that the model's critical pole reaches maximum damping at a gain between -0.002 and -0.003, consistent with the optimum predicted gain of -0.0025 indicated in Figure 8, whereas the corresponding identified pole's damping peaks at a gain of about -0.005.

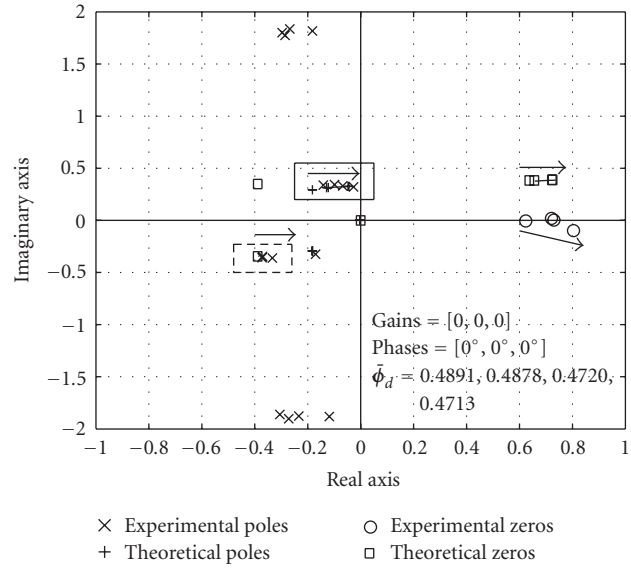

Figure 9: Open-loop root locus for harmonic 1 with varying flow coefficient.

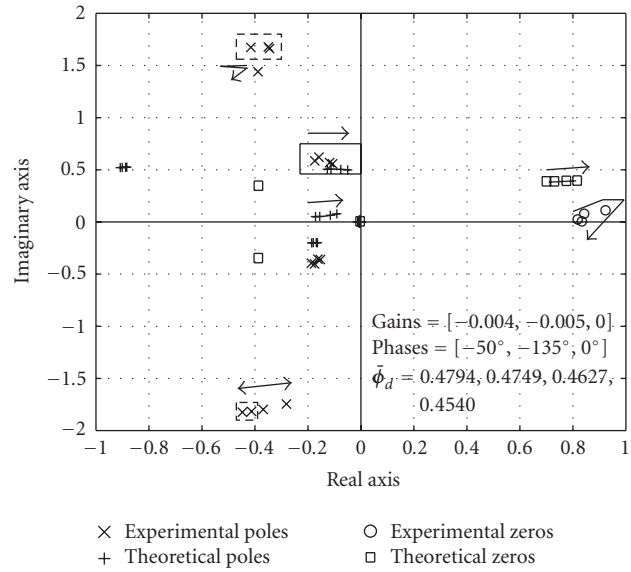

Figure 10: Closed-loop root locus for harmonic 1 with varying flow coefficient.

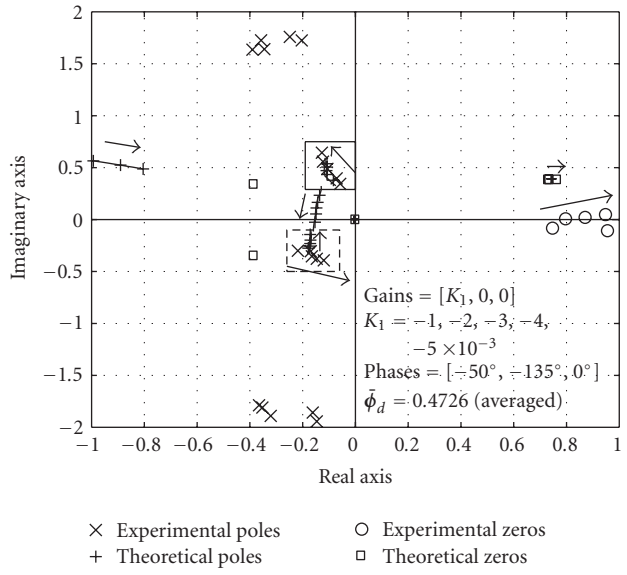

Figure 11: Closed-loop root locus for harmonic 1 with varying gain.

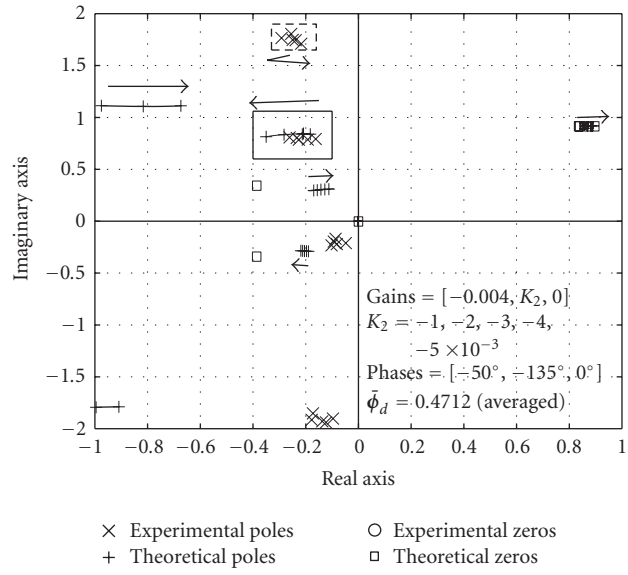

Figure 12: Closed-loop root locus for harmonic 2 with varying gain.

As for harmonic 2, Figure 12 shows that the increase in damping of the precursor pole with gain is lower than that predicted by the model. Similarly, the root loci with respect to the controller phase, depicted in Figures 13 and 14, show that the model predicts the general trajectory of the precursor pole with varying controller phase correctly, although the error in the prediction of the position of the critical pole is larger than that for the case of varying gain.

The above observations suggest that the model is qualitatively accurate in terms of predicting the dynamic behavior

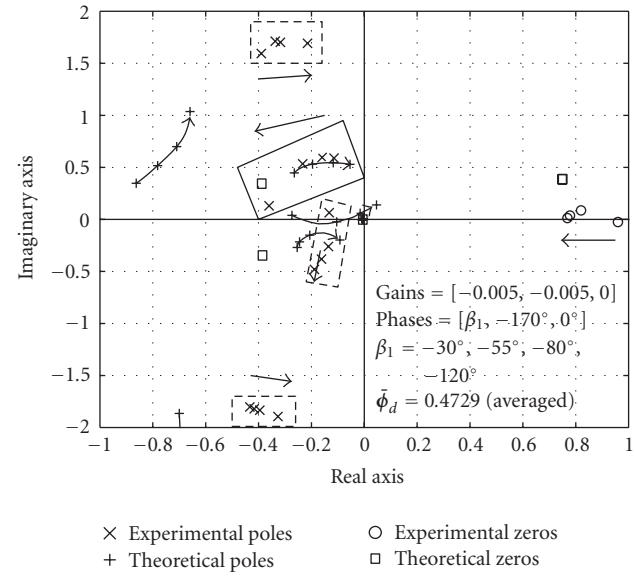

Figure 13: Closed-loop root locus for harmonic 1 with varying phase.

associated with the stall precursor pole, which according to theory is the critical pole leading to rotating stall. As such, the model is useful in designing compensators to counter undesirable effects such as the migration of the first harmonic precursor pole into the high frequency zone. However, the overestimation of the damping of the critical pole, especially with respect to varying gain in the case of the second spatial harmonic (see Figure 12), suggests that the compressor, with closed-loop active control, will stall at a higher flow coefficient than predicted. In addition, slight inaccuracies in the detailed trajectory of the critical pole would indicate that the predicted optimum controller gain and phase will be slightly off.

5. ACTIVE CONTROL EXPERIMENTS

Active control experiments with jet actuation and proportional feedback control are performed to quantitatively compare the model's stall predictions with real values. During experimental tuning of the controller's gain and phase for the first three spatial harmonics, the flow coefficient downstream of the compressor at stall is recorded for several values of gain and phase that can be compared with theoretical predictions. The experimentally optimized controller gains and phases are then used to assess the maximum flow range extension achievable on this compressor with distributed jet actuation and closed-loop control.

5.1. Experimental procedure

The tuning experiments are carried out at a mean injection rate of 9.3% of the stalling mass flow of the reference baseline (no control/no blowing) case by slowly throttling the compressor into stall starting with first harmonic control. First,

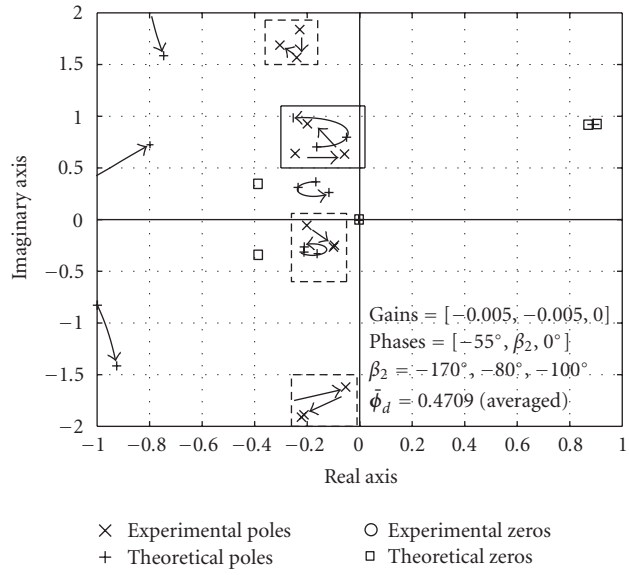

Figure 14: Closed-loop root locus for harmonic 2 with varying phase.

fixing the feedback phase at a value close to the theoretically predicted optimal phase, the system is stalled at different feedback gains. Once an optimum gain is chosen and fixed, the procedure is repeated with varying phase to find the optimum phase value. Subsequently, with the compressor under first harmonic feedback control at the optimum gain and phase, the control parameters for the second harmonic are tuned in the same manner, and so on.

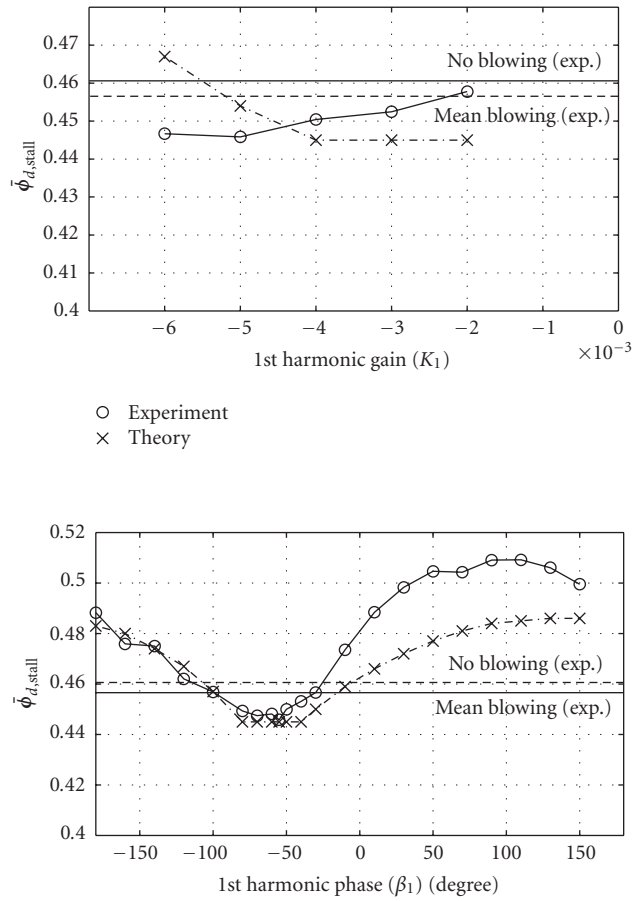

Figure 15: Experimental gain and phase optimization for first harmonic control. Top: gains = $[K_1, 0, 0]$ and phases = $[-55°, 0°, 0°]$. Bottom: gains = $[-0.005, 0, 0]$ and phases = $[\beta_1, 0°, 0°]$.

5.2. Controller tuning results

Figures 15 and 16 present the results from experimental controller gain and phase tuning for the first and second spatial harmonics, respectively. The experimental stall flow coefficients and the corresponding predicted stall flow coefficients for the first two spatial harmonics for different feedback gains and phases are shown in the upper and lower plots, respectively. To highlight the effect of closed-loop control of each additional harmonic, the measured stalling flow coefficients for two reference cases are indicated by the horizontal lines on each plot. The first reference case is a run without blowing/control. For first harmonic control tuning (see Figure 15), the second reference case involves mean blowing without control. For second harmonic control tuning (see Figure 16), the second reference case has mean blowing and experimentally optimized first harmonic control.

Figure 15 suggests that the model accurately predicts the effect of feedback phase on the system for first spatial harmonic control. However, it is completely off in predicting the optimum gain of about −0.0025 compared to the actual value between −0.004 and −0.005. This is consistent with Figure 11, which shows the theoretical critical pole attaining maximum damping of the critical pole at gain values between −0.002 and −0.003, while the experimental critical pole reaches maximum damping at a gain of around −0.005. For the second harmonic (see Figure 16), the predicted trends are approximately correct for the feedback gain and phase but the values are off. It must be noted that measurement problems were encountered for the run with a gain of −0.003 in the upper plot of Figure 16 and that this point should thus be ignored.

Tuning results for the third harmonic (with optimized first and second harmonic control) are not presented here because they do not show any significant changes in stalling flow coefficient with varying third harmonic feedback gain and phase. This is consistent with the model's prediction that stall with first and second harmonic control is not due to the critical pole of the third harmonic but rather to the failure to better damp the critical pole of the first harmonic.

Based on the tuning experiments, the optimum feedback gains and phases for the first three spatial harmonics are picked, respectively, as $[-0.005, -0.005, -0.004]$ and $[-55°, 170°, 160°]$.

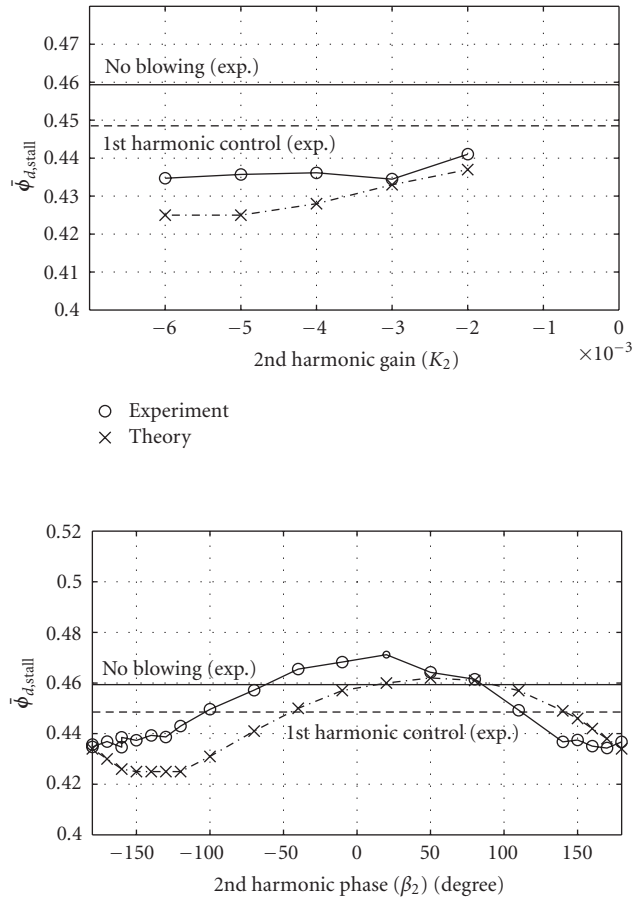

FIGURE 16: Experimental gain and phase optimization for second harmonic control. Top: gains = $[-0.005, K_2, 0]$ and phases = $[-55^\circ, -180^\circ, 0^\circ]$. Bottom: gains = $[-0.005, -0.005, 0]$ and phases = $[-55^\circ, \beta_2, 0^\circ]$.

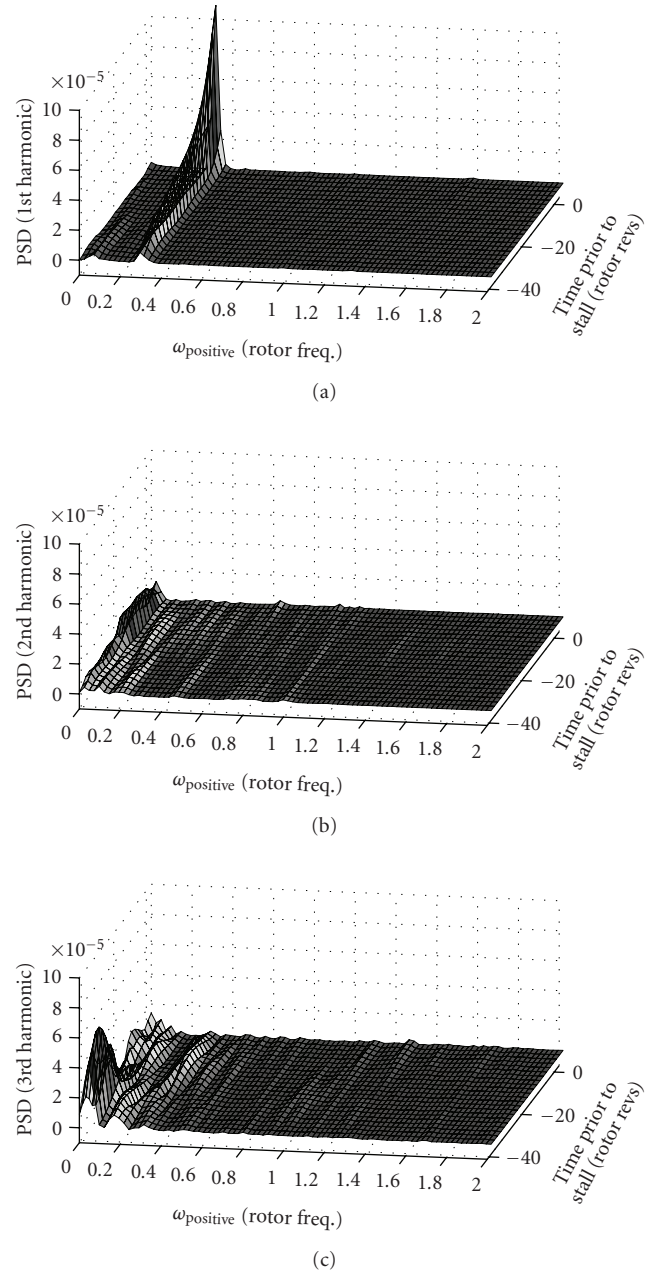

FIGURE 17: PSD of first three spatial harmonics of measured prestall disturbance with mean blowing and no control (positive rotating frequencies).

5.3. Optimized closed-loop control

Control experiments using the empirically optimized control parameters are subsequently carried out. All runs are performed twice to insure repeatability. The results show that the stall flow coefficient is repeatable to within ± 0.001 in most cases and ± 0.002 in some cases. Figures 17 through 19 show the power spectral density (PSD) of the velocity perturbations at the first rotor face for the first three harmonics. The PSD was obtained from hot-wire measurements at stall inception (within 40 rotor revolutions prior to stall), multiplied by a factor to account for the exponential decay of the modal disturbances between the first rotor face and the location of the hot wires. For conciseness, only the region of (positive) rotating frequencies in the direction of the rotor (positive imaginary axis of the root locus plots), where there is disturbance growth, is shown. Figure 17 represents the reference case with mean blowing but without control, clearly showing the growth of the first harmonic perturbation as the stall precursor, rotating at around 30% of rotor speed, which corresponds to the critical pole in Figure 9. These results are similar to those of the baseline case without mean blowing (not shown).

In Figure 18, with first harmonic control, the growth of the first harmonic perturbation is clearly suppressed, while it is now at around 50% rotor speed as expected from the upward movement of the critical pole with closed-loop control in Figures 10 and 11. In this case, it is the second harmonic perturbation at around 80% rotor speed, corresponding to the critical pole in Figure 12, which grows into stall, as predicted by the model. A range extension of 2.4% in terms of

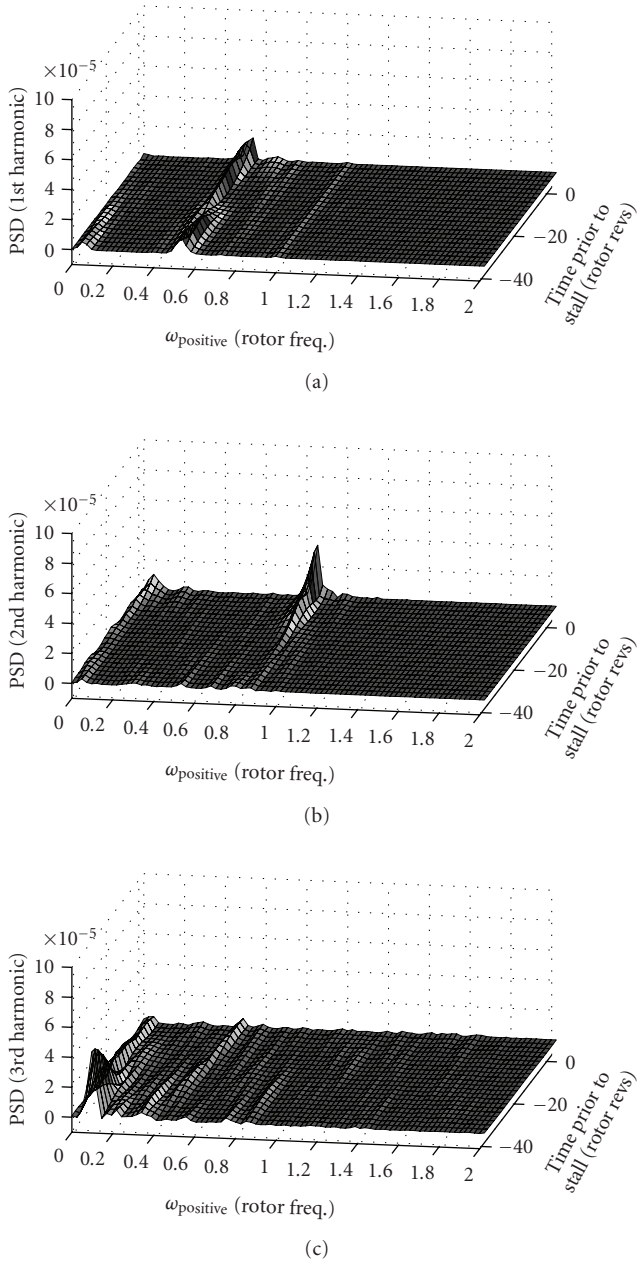

Figure 18: PSD of first three spatial harmonics of measured prestall disturbance with first harmonic control (positive rotating frequencies).

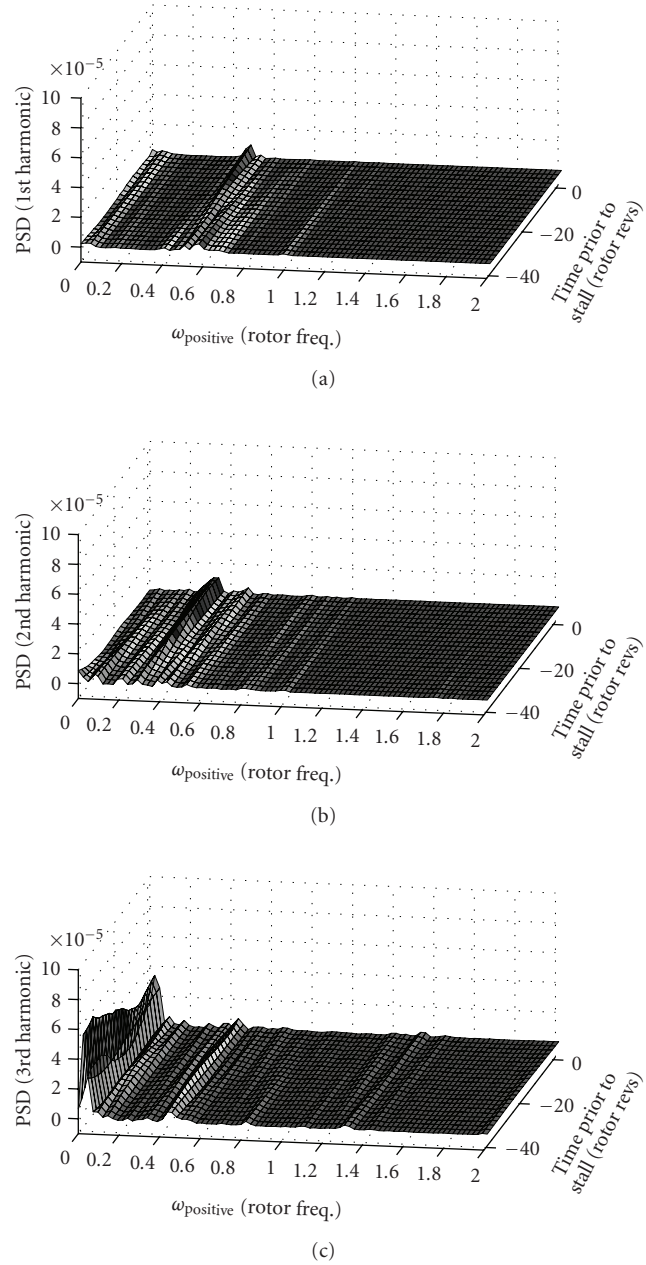

Figure 19: PSD of first three spatial harmonics of measured prestall disturbance with first and second harmonic control (positive rotating frequencies).

flow coefficient at stall is achieved with respect to the baseline (no blowing) case. The model of the system with real injection and external dynamics predicts the same range extension.

The application of both first and second harmonic control increases the range extension to 4.8%, compared to a model prediction of 6.8%. This model's over-prediction is expected because of its overestimation of damping with varying gain as observed in Figure 12. In this case, although the model predicts that stall would occur due to the first harmonic perturbation, the PSD plots in Figure 19 do not show any clear growth for the first three harmonics. Concerning the large, though nongrowing third harmonic disturbance at low rotating speed, it may be noise multiplied by the amplification factor to account for the higher upstream decay rate of higher spatial harmonic disturbances. This decay makes the measurements less reliable for the third harmonic and unreliable for higher harmonics (decayed perturbation amplitude at hot-wire location below noise levels).

Last but not least, the model predicts no gain from the addition of third harmonic control, and measurement shows only a little gain, giving a maximum improvement in

Table 1: Summary of experimental and theoretical stall flow coefficients with optimized closed-loop control.

Downstream flow coefficient at stall ($\overline{\phi}_{d,\text{stall}}$) [% decrease in $\overline{\phi}_{d,\text{stall}}$ from baseline]				
Description	Experiment	Model w/o feedback dynamics and ideal injection	Model w/o feedback dynamics and real injection	Model with feedback dynamics and real injection
No blowing (baseline)	0.458	0.456	0.456	0.456
Mean blowing, no control	0.455 [0.7%]	0.454 [0.4%]	0.461 [−1.1%]	0.461 [−1.1%]
1st harmonic control	0.447 [2.4%]	0.436 [4.3%]	0.445 [2.4%]	0.445 [2.4%]
1st and 2nd harmonic control	0.436 [4.8%]	0.402 [11.8%]	0.414 [9.2%]	0.425 [6.8%]
1st, 2nd, and 3rd harmonic control	0.433 [5.5%]	0.385 [15.6%]	0.409 [10.3%]	0.425 [6.8%]

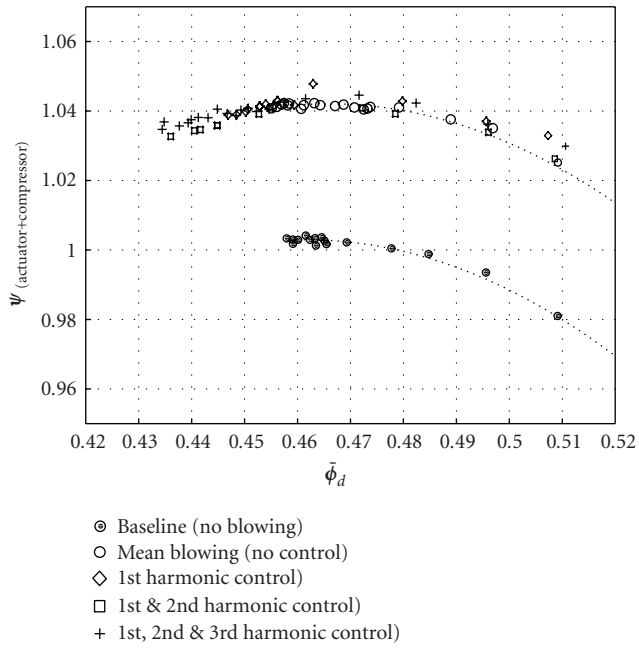

Figure 20: Actuator/compressor total-to-stagnation pressure rise characteristics (speedlines) with and without optimized constant feedback control.

downstream stall flow coefficient of 5.5% with respect to the baseline case. As in the case with first and second harmonics control, the PSD plots for this case (not shown) do not indicate any clear growth in the first three spatial harmonics.

The above results are summarized in Figure 20, which shows the effect of active control with distributed jet actuation on the pressure rise characteristics of the compressor, as well as in Table 1, which compares experimental range extension with optimal theoretically predicted values with various levels of modeling. As expected, the models with ideal injection and/or no feedback dynamics largely overestimate the effectiveness of closed-loop control with jet injection, in term of percentage reduction in stalling flow coefficient. This highlights the importance of incorporating feedback dynamics in the model of the closed-loop system.

6. CONCLUSION

The effectiveness of distributed jet actuation in active suppression of modal stall inception in a low speed multistage axial compressor is analytically and experimentally evaluated. Detailed modeling of jet actuation indicates that although momentum addition is still the main effect, mass addition can significantly reduce the effective pressure rise from jet actuation, and by extension, the effectiveness of the actuators. Moreover, practical considerations such as discrete actuators and associated nonideal mixing reduce the effective pressure rise imparted by the jet as the flow coefficient is reduced. The above effects should be considered when designing jet injection for flow control. The integration of an updated empirical model for injection into a Moore-Greitzer compressor model with unsteady losses shows that the effect of nonideal injection is to reduce the stall range extension by about the same proportion as the reduction in effective pressure rise due to the jet. In addition, the presence of feedback (external) dynamics in the control loop can result in a dramatic drop in range extension and thus should be accounted for in any theoretical studies and controller design using jet actuation.

System identification experiments indicate that the complete model of the closed-loop system with real injection characteristics and feedback dynamics is qualitatively correct in predicting the location and movement of the critical pole. Hence, the model constitutes a very useful tool to design control laws that move the critical pole in the desirable direction of higher damping and lower rotational frequency. Clearly, with the presence of feedback dynamics in this system, proportional feedback control is inadequate as it puts stress on the bandwidth of the actuator by moving the critical pole of the first spatial harmonic disturbance toward a higher rotational speed rather than toward higher damping, as the gain is increased. Better controller design should eliminate the effect of control system dynamics, where upon the limitation in range extension of the compressor under closed-loop control should rest on the effectiveness of the jet injectors.

Analysis of the prestall disturbances from active control experiments show a behavior of the stall precursor that is consistent with the location and movement of the critical pole predicted by the model and system identification,

especially for control of the lower spatial harmonics. In terms of stall delay, the trends are right but, as expected from the over prediction of the damping by the model, the stall predictions are slightly optimistic. The best result achieved with jet actuation in this system with proportional feedback control is a range extension of 5.5% in downstream flow coefficient compared with a theoretically predicted maximum of 6.8%. However, a more sophisticated controller that can mitigate the negative effects of the feedback dynamics could improve the range extension with this actuation scheme.

NOMENCLATURE

Symbols

A: Area
$A(s)$: Actuator dynamics
$D(s)$: Feedback time delay transfer function
$F(s)$: Butterworth filter transfer function
f: Cut-off frequency of $F(s)$
K_n: Controller feedback gain
L_u: Pressure loss across the compressor due to viscous losses
L_{uR}: Pressure loss across the rotors due to viscous losses
L_{uS}: Pressure loss across the stators due to viscous losses
$\dot{m}$: Mass flow
n: harmonic number
P_t: Total pressure
P_s: Static pressure
PSD: Power spectral density
R: Mean compressor radius
r: Compressor reaction
s: Laplace transform variable
t: Time
U: Mean rotor blade velocity
$ZOH(s)$: Discrete sampling dynamics transfer function
α: Injection angle in the annular plane with respect to axial direction
β_n: Controller feedback phase
γ: Injection angle in the radial plane with respect to axial direction
η: Nondimensional axial position with respect to compressor face
λ: Rotor fluid inertia
μ: Total fluid inertia in the compressor
ρ: Air density
ξ: Nondimensional time
Φ: Local flow potential
ϕ: Axial flow coefficient, $(\textit{axial velocity})/U$
$\overline{\phi}$: annulus-averaged axial flow coefficient
ξ: Nondimensional time
τ_a: Jet convection time lag constant
τ_f: Sampling ($ZOH(s)$) time constant
τ_t: Feedback delay ($D(s)$) time constant
ω: Temporal frequency
ϕ_n: nth spatial Fourier coefficient of flow coefficient disturbance $\delta\phi$
$\overline{\phi}_d$: $\overline{\phi}$ downstream of the jet actuator
ψ: Steady-state stagnation-to-static pressure rise coefficient, $(P_{s,\text{out}} - P_{t,\text{in}})/\rho U^2$
ψ_i: Steady-state isentropic stagnation-to-static pressure rise coefficient
ψ_{jet}: Stagnation pressure rise coefficient due to jet actuation

Operator, superscripts, and subscripts

$\delta(\ )$: Small perturbation
$(\sim)$: Spatial Fourier coefficient
$(\bullet)$: Derivative with respect to nondimensional time (ξ)
$(\ )^*$: Complex conjugate
$(\ )_c$: Pertaining to the input
$(\ )_I$: Station (i) in Figure 5
$(\ )_j$: Pertaining to the jet
$(\ )_n$: nth harmonic
$(\ )_{\text{hw}}$: Hot wires
$(\ )_u$: Upstream of actuator
$(\ )_d$: Downstream of actuator
$(\ )_{,ss}$: Steady state

ACKNOWLEDGMENTS

This work was carried out while the author was at the Gas Turbine Laboratory, Massachusetts Institute of Technology, Cambridge, MA. The author wishes to thank Dr. J. D. Paduano, Professor A. H. Epstein, and Dr. H. J. Weigl for their advice, and Dr. J. Protz, Dr. C. Van Schalkwyk and the technicians of the MIT Gas Turbine Laboratory for their help in setting up the experimental facilities. This work was sponsored by the U.S. Air Force Office of Scientific Research, Dr. J. McMicheal, Technical Manager, whose support is gratefully acknowledged.

REFERENCES

[1] I. J. Day, "Stall inception in axial flow compressors," *Journal of Turbomachinery*, vol. 115, no. 1, pp. 1–9, 1993.
[2] C. Nie, G. Xu, X. Cheng, and J. Chen, "Micro air injection and its unsteady response in a low-speed axial compressor," *Journal of Turbomachinery*, vol. 124, no. 4, pp. 572–579, 2002.

[3] H. D. Vo, C. S. Tan, and E. M. Greitzer, "Criteria for spike initiated rotating stall," in *Proceedings of the ASME Turbo Expo—Gas Turbie Technology: Focus for the Future*, pp. 155–165, Reno-Tahoe, Nev, USA, June 2005, ASME Paper GT2005-68374.

[4] F. K. Moore, "Theory of rotating stall of multistage axial compressors—part I: small disturbances—part II: finite disturbances—part III: limit cycles," *Journal of Engineering for Gas Turbines and Power*, vol. 106, no. 2, pp. 313–336, 1984.

[5] F. K. Moore and E. M. Greitzer, "Theory of post-stall transients in axial compression systems—part I: development of equations," *Journal of Engineering for Gas Turbines and Power*, vol. 108, no. 1, pp. 68–76, 1986.

[6] J. D. Paduano, A. H. Epstein, L. Valavani, J. P. Longley, E. M. Greitzer, and G. R. Guenette, "Active control of rotating stall in a low-speed axial compressor," *Journal of Turbomachinery*, vol. 115, no. 1, pp. 48–56, 1993.

[7] J. M. Haynes, G. J. Hendricks, and A. H. Epstein, "Active stabilization of rotating stall in a three-stage axial compressor," *Journal of Turbomachinery*, vol. 116, no. 2, pp. 226–239, 1994.

[8] C. M. Van Schalkwyk, J. D. Paduano, E. M. Greitzer, and A. H. Epstein, "Active stabilization of axial compressors with circumferential inlet distortion," *Journal of Turbomachinery*, vol. 120, no. 3, pp. 431–439, 1998.

[9] G. J. Hendricks and D. L. Gysling, "Theoretical study of sensor-actuator schemes for rotating stall control," *Journal of Propulsion and Power*, vol. 10, no. 1, pp. 101–109, 1994.

[10] D. L. Gysling and E. M. Greitzer, "Dynamic control of rotating stall in axial flow compressors using aeromechanical feedback," *Journal of Turbomachinery*, vol. 117, no. 3, pp. 307–319, 1995.

[11] H. J. Weigl, J. D. Paduano, L. G. Fréchette, et al., "Active stabilization of rotating stall and surge in a transonic single-stage axial compressor," *Journal of Turbomachinery*, vol. 120, no. 4, pp. 625–636, 1998.

[12] K. L. Suder, M. D. Hathaway, S. A. Thorp, A. J. Strazisar, and M. B. Bright, "Compressor stability enhancement using discrete tip injection," *Journal of Turbomachinery*, vol. 123, no. 1, pp. 14–23, 2001.

[13] R. D'Andrea, R. L. Behnken, and R. M. Murray, "Rotating stall control of an axial flow compressor using pulsed air injection," *Journal of Turbomachinery*, vol. 119, no. 4, pp. 742–752, 1997.

[14] S. Yeung, Y. Wang, and R. M. Murray, "Bleed valve rate requirements evaluation in rotating stall control on axial compressors," *Journal of Propulsion and Power*, vol. 16, no. 5, pp. 781–791, 2000.

[15] Z. S. Spakovszky, J. D. Paduano, R. Larsonneur, A. Traxler, and M. M. Bright, "Tip clearance actuation with magnetic bearings for high-speed compressor stall control," *Journal of Turbomachinery*, vol. 123, no. 3, pp. 464–472, 2001.

[16] M. T. Schobeiri and M. Attia, "Active control of compressor instability and surge by stator blades adjustment," *Journal of Propulsion and Power*, vol. 19, no. 2, pp. 312–317, 2003.

[17] L. G. Fréchette, O. G. McGee, and M. B. Graf, "Tailored structural design and aeromechanical control of axial compressor stall—part II: evaluation of approaches," *Journal of Turbomachinery*, vol. 126, no. 1, pp. 63–72, 2004.

[18] H. D. Vo and J. D. Paduano, "Experimental development of a jet injection model for rotating stall control," in *Proceedings of the International Gas Turbine & Aeroengine Congress & Exhibition*, p. 11, Stockholm, Sweden, June 1998, ASME Paper 98-GT-308.

[19] D. S. Diaz, "Design of a jet actuator for active control of rotating stall," S.M. thesis, Department of Aeronautics and Astronautics, MIT, Cambridge, Mass, USA, 1994.

[20] A. H. J. Eastland, "Investigation of compressor performance in rotating stall," MIT GTL Report 164, MIT, Cambridge, Mass, USA, 1982.

[21] R. N. Gamache and E. M. Greitzer, "Reverse flow in multistage axial compressors," *Journal of Propulsion and Power*, vol. 6, no. 4, pp. 461–473, 1990.

[22] V. H. Garnier, A. H. Epstein, and E. M. Greitzer, "Rotating waves as a stall inception indication in axial compressors," *Journal of Turbomachinery*, vol. 113, no. 2, pp. 290–302, 1991.

[23] J. D. Paduano, "Active control of rotating stall in axial compressors," MIT GTL Report 208, MIT, Cambridge, Mass, USA, 1992.

[24] J. M. Haynes, "Active control of rotating stall in a three-stage axial compressor," MIT GTL Report 218, MIT, Cambridge, Mass, USA, 1993.